

Article

Experimental Dataset of Tunable Mode Converter Based on Long-Period Fiber Gratings Written in Few-Mode Fiber: Impacts of Thermal, Wavelength, and Polarization Variations

Juan Soto-Perdomo ¹, Erick Reyes-Vera ^{1,*}, Jorge Montoya-Cardona ² and Pedro Torres ³

¹ Department of Electronics and Telecommunications, Instituto Tecnológico Metropolitano, Medellín 050034, Colombia; juansoto319998@correo.itm.edu.co

² Departamento de Óptica, Centro de Investigación Científica y de Educación Superior de Ensenada, Ensenada 22860, BC, Mexico; montoyacj@cicese.edu.mx

³ Escuela de Física, Universidad Nacional de Colombia, Medellín 050034, Colombia; pitorres@unal.edu.co

* Correspondence: erickreyes@itm.edu.co

Abstract: Mode division multiplexing (MDM) is currently one of the most attractive multiplexing techniques in optical communications, as it allows for an increase in the number of channels available for data transmission. Optical modal converters are one of the main devices used in this technique. Therefore, the characterization and improvement of these devices are of great current interest. In this work, we present a dataset of 49,736 near-field intensity images of a modal converter based on a long-period fiber grating (LPFG) written on a few-mode fiber (FMF). This characterization was performed experimentally at various wavelengths, polarizations, and temperature conditions when the device converted from LP₀₁ mode to LP₁₁ mode. The results show that the modal converter can be tuned by adjusting these parameters, and that its operation is optimal under specific circumstances which have a great impact on its performance. Additionally, the potential application of the database is validated in this work. A modal decomposition technique based on the particle swarm algorithm (PSO) was employed as a tool for determining the most effective combinations of modal weights and relative phases from the spatial distributions collected in the dataset. The proposed dataset can open up new opportunities for researchers working on image segmentation, detection, and classification problems related to MDM technology. In addition, we implement novel artificial intelligence techniques that can help in finding the optimal operating conditions for this type of device.

Keywords: optical mode conversion; long-period fiber grating; mode division multiplexing; optical fiber; few-mode fiber



Citation: Soto-Perdomo, J.; Reyes-Vera, E.; Montoya-Cardona, J.; Torres, P. Experimental Dataset of Tunable Mode Converter Based on Long-Period Fiber Gratings Written in Few-Mode Fiber: Impacts of Thermal, Wavelength, and Polarization Variations. *Data* **2024**, *9*, 10. <https://doi.org/10.3390/data9010010>

Academic Editors: Vladimir Sreckovic and Giuseppe Ciaburro

Received: 8 November 2023

Revised: 19 December 2023

Accepted: 30 December 2023

Published: 31 December 2023



Copyright: © 2023 by the authors. Licensee MDPI, Basel, Switzerland. This article is an open access article distributed under the terms and conditions of the Creative Commons Attribution (CC BY) license (<https://creativecommons.org/licenses/by/4.0/>).

1. Introduction

The demand for data transmission over optical links continues to grow, and requires the development of new optical communication technologies to overcome the capacity limit that is about to be reached worldwide. Different techniques, such as time division multiplexing (TDM), wavelength division multiplexing (WDM), and polarization division multiplexing (PDM), have been implemented in modern single-mode fiber-based communication systems. Currently, WDM coherent optical communication systems have maximized the utilization of degrees of freedom, specifically frequency, quadrature, and polarization. As a result, the spatial dimension emerges as the only additional parameter that can be used in optical fiber communication systems, giving rise to the technology of spatial division multiplexing (SDM), with which independent data streams can be transmitted in parallel spatial channels in SDM systems. SDM can be implemented in one of two ways. The first uses Multi-Core Fibers (MCF), with each core acting as an independent channel for information transmission [1–4]. It is worth saying that we generally distinguish between weakly coupled MCFs, where signal interactions between cores are usually undesirable,

and coupled-core MCFs, where a smaller core pitch leads to a stronger intentional random coupling of signals in different cores. The second technique is Modal Division Multiplexing (MDM), in which the spatial modes in few-mode fiber are exploited as independent transmission channels; in this case, the capacity of a fiber increases with the number of spatial modes available for multiplexing.

Mode multiplexers (MUX) and demultiplexers (DEMUX) play key roles in switching single-mode parallel fibers (SMFs) signals to SDM signals with an overlap of distinct modes for effective SDM transmission. Each MUX consists of two parts: a mode converter and a combiner. As a result, the design of mode converters to assist in the conversion and control of the propagating modes in an optical fiber becomes critical for the proper implementation of this technology. Modal converters are devices that convert a particular spatial mode in a fiber into another spatial mode. These devices are now important parts of transmission systems, and need to be carefully designed to have the right number of modes, low crosstalk between modes, high mode-conversion efficiency, or wide operating bandwidth, depending on the method [5,6]. Because of this, numerous research efforts have been directed toward the development of high-performance mode converters, and several types of mode converters have been demonstrated with bulk-optic components [7–10], optical fibers [11–17], and optical waveguides [18–20]. Bulk-optic mode converters require critical alignment and have a large insertion loss. To overcome these problems, several fiber mode converters (using mode-selective directional couplers [1–3,21] and long-period gratings (LPGs) [22–24]) and waveguide mode converters (using Y-junctions [25], Mach-Zehnder interferometers [26,27], LPGs [18,19], etc.) have been proposed. Among these, LPFGs are particularly simple and flexible structures for the design and implementation of mode converters [28].

For example, Sakata et al. reported a tunable fiber mode converter utilizing an LPFG (which is crucial for the device's operation) induced by periodic microbends in the optical fiber using an electromagnet [22]. The results showed that this device allows the conversion of the fundamental mode to the LP_{11} mode according to the voltage provided to the electromagnet. In 2016, Zhao et al. reported the fabrication of inclined LPFGs fabricated in two-mode fiber (TMF) using the CO_2 laser method [23]. They demonstrated that the coupling between LP_{01} mode and LP_{11} mode can be adjusted by changing the tilt angle. Two years later, Liu and his colleagues showed a new way to change the polarization of light to create orbital angular momentum (OAM) of ± 1 -order in LPFGs [29]. The authors utilized the superposition of the LP_{11} modes to generate the OAM modes. Furthermore, they provided evidence that the OAM vortex phase of the produced modes remained unchanged as the temperature rose from 23 °C to 50 °C. In 2021, Zheng et al. demonstrated a wavelength-tunable mode converter based on an LPFG [30]. To do this, they first created adiabatic tapers with cladding diameters of 113 μm and 121 μm , then the LPFGs were written in the optical fiber taper in such a way that modal conversion between LP_{01} and LP_{11} modes was generated. Finally, they demonstrated that adjusting the operational wavelength of the light source allowed the response of the modal converter to be tuned. They used a CCD camera to demonstrate the presence of multiple modes at different wavelengths based on changes in the spatial distribution of the intensity. Modal converters are sensitive to changes in parameters such as temperature, strain, wavelength, and polarization, among others. However, no study examining the fluctuation of two or more of these parameters simultaneously has been performed. As a result, a database containing this information would be needed in order to optimize this kind of device.

In addition to the requirement that the mode-selective devices used in an MDM system should be able to operate the WDM signal over the entire (C + L) band (from 1530 nm to 1610 nm), there is a need to use sophisticated adaptive multiple-input multiple-output (MIMO) processing schemes for spatial demultiplexing in order to exploit the full capability of MDM. Approaches for mode demultiplexing with reduced complexity, even for few-mode MDM, are of great interest for both telecommunications and other applications [31].

The growing interest in mode-selective devices stimulates the demand for efficient mode characterization algorithms at the mode-selective device output. Several methods have been proposed for this purpose. Numerical computing-based methods include the classical Gerchberg–Saxton technique [32], mode decomposition [31,33], the fractional Fourier system [34], and machine learning methods [31,35,36]. However, previously published results are very limited in terms of the number of modes, and are characterized by a relatively long processing time. For example, Yan et al. proposed a method based on a deep learning approach to characterize degenerate optical modes in FMF [33]. They retrieved the modal coefficients using three polarization projection images, and a well-trained deep convolutional neural network (CNN) demonstrated efficient learning of the mapping relationship from a two-dimensional intensity distribution to a one-dimensional coefficient space of eigenmodes. Evaluation criteria such as modal coefficient errors and average image correlation showed encouraging results, with coefficient errors under 1% and correlation over 95%. On the other hand, Manuilovich et al. presented a non-iterative algorithmic method for MD in FMFs in the absence of a reference beam [31]. For three-, five-, and eight-mode fibers, the proposed method reached decomposition speeds of up to 100,000 frames per second, making it the fastest intensity-only MD method to date. Likewise, the experiment demonstrated its applicability to MD in a 27-mode fiber, showcasing the algorithm’s stability under various noise levels in the input signals. While a few researchers have used experimental data [31,36], most authors of MD algorithms have validated them using simulated data [33,37]. In many cases, these simulated datasets lack challenges associated with noise or experimental difficulties, making it difficult to optimize methods in real-world scenarios. As a result, databases that examine a variety of experimental conditions and their possible impact on the propagation of optical modes could substantially contribute to this research area.

In this work, we evaluate the response of an LPFG mode converter to various experimental situations, such as the impact of input polarization, output polarization, and operating wavelength, as well as how the modal converter can be tuned by changing the temperature. This dataset serves a multitude of purposes, including training, testing, and validation of various computational models related to object detection, image segmentation techniques, optimization techniques, modal prediction, etc. As a direct application, we have leveraged this dataset, employing a modal decomposition technique using an optimization algorithm to estimate modal amplitudes and phases, which are key elements for optimizing modal conversion techniques that make use of LPFGs. These labels not only offer the possibility to refine and improve modal conversion processes, they provide a solid basis for integration with artificial intelligence models. This direct application underlines the practical utility and relevance of the database, demonstrating its contribution to theoretical advancement as well as to the effective implementation of modal decomposition techniques in the field of fiber optics.

2. Methods

2.1. LPFG-Based Modal Converter Principle

LPFGs are made by introducing a periodic perturbation to the refractive index of the fiber, allowing for energy exchange between different propagation modes. Coupled Mode Theory (CMT) is the widely accepted approach to analyzing waveguides with small perturbations [38]. It involves solving a system of coupled differential equations and determining the coupling coefficients that govern the transfer of optical power between the different modes supported by the optical fiber.

The electromagnetic field of the LP₀₁ and LP₁₁ modes can be expressed in the forms

$$\begin{aligned}\vec{E}_{01}(x, y, z) &= a_{01}(z) \vec{E}_{01}(x, y) e^{-i\beta_{01}z} \\ \vec{E}_{11}(x, y, z) &= a_{11}(z) \vec{E}_{11}(x, y) e^{-i\beta_{11}z},\end{aligned}\tag{1}$$

where $a_{i1}(z)$ are known as expansion coefficients and represent the electric field amplitude of the propagation modes in the fiber core, while β_{01} and β_{11} correspond to the propagation constants of the modes LP₀₁ and LP₁₁, respectively. In a pristine optical fiber, these modes are not coupled and the expansion coefficients $a_{i1}(z)$ are constants that are independent of the direction of propagation z . When there is a spatially dependent disturbance in the optical fiber, the modes defined by the fiber are no longer orthogonal modes and can now be coupled by the disturbance as they propagate along the fiber. As a result, the expansion coefficients are no longer propagation constants, and vary with z as the fields propagate through the fiber.

In the case of the LPFG studied in this work, the two guided modes propagate in the same direction ($+z$); consequently, the propagation constants associated with the two guided modes have positive values. Therefore, the equations describing the coupling between the LP₀₁ and LP₁₁ modes are as follows:

$$\begin{aligned}\frac{da_{01}(z)}{dz} &= -i\beta_{01}a_{01}(z) - i\kappa a_{11}(z)e^{-i(\beta_{01}-\beta_{11}+K)z} \\ \frac{da_{11}(z)}{dz} &= -i\beta_{11}a_{11}(z) - i\kappa a_{01}(z)e^{i(\beta_{01}-\beta_{11}+K)z},\end{aligned}\quad (2)$$

where $K = 2\pi/\Lambda$ is the wave vector of the grating, Λ is the LPFG period, and κ is the coupling coefficient between LP₀₁ mode and the LP₁₁ mode, which is provided by

$$\kappa(z) = \frac{\omega}{4} \iint \vec{E}_{01}^*(x,y)\Delta\varepsilon(x,y)\vec{E}_{11}(x,y)dxdy.\quad (3)$$

Here, ω is the angular frequency, while $\vec{E}_{01}(x,y)$ and $\vec{E}_{11}(x,y)$ are the electric field distributions of the LP₀₁ and LP₁₁ modes, respectively. Likewise, $\Delta\varepsilon(x,y)$ denotes the perturbation in the refractive index profile of the optical fiber. Equation (2) illustrates the rate of change of the amplitude of the i^{th} mode depends on the amplitudes of the coupled modes within the LPFG and the phase difference between them. According to the phase-matching condition, significant power exchange in the LPFG occurs when $\beta_{01} - \beta_{11} + K = 0$, which can be expressed in terms of effective refractive indices and wavelength, as follows:

$$\Lambda = \frac{\lambda_{\text{res}}}{n_{\text{eff},01} - n_{\text{eff},11}},\quad (4)$$

where λ_{res} is the resonance wavelength of the LPFG. It is crucial to highlight that this resonant wavelength can be tuned through strain or temperature effects [2,22,23,39].

2.2. Mode Converter Fabrication

Figure 1 illustrates the LPFG engraving system. The proposed system employs a CO₂ laser (Iradion, Infinity Series: Model 155) with a maximal rated optical power of 160 W, a beam diameter of 2.5 mm, a beam divergence of 5.2 mrad, and a laser pulse frequency of 5 kHz. The LPFG in this work was created using a laser power of 14.5 W and an irradiation time of 600 ms. A ZnSe cylindrical lens with a focal length of 50 mm was used to focus the laser beam to the optical fiber core (SM2000, Thorlabs, Newton, NJ, USA), obtaining a spot size of 150 μm . During the LPFG inscription process, one end of the few-mode fiber was securely clamped in a translational stage fiber holder, while the other end was attached to a small weight (~ 20.1 g) to provide a constant pre-tension in the optical fiber, greatly improving the LPFG inscription efficiency [39].

The entire procedure, encompassing crucial grating characteristics such as pitch, the number of grating periods, and the quantity of scanning cycles, was skillfully configured using the user-friendly interface of a PC operating system, as detailed in our previous research [39,40]. In this work, the CO₂ laser beam advanced along the fiber in steps to repeat the transverse scanning process with a pitch $\Lambda = 570$ μm . A scanning cycle was completed when 50 periods had elapsed. Consequently, the laser beam induced an

asymmetric refractive-index distribution across the fiber core, enabling energy coupling between LP_{01} mode and LP_{11} mode.

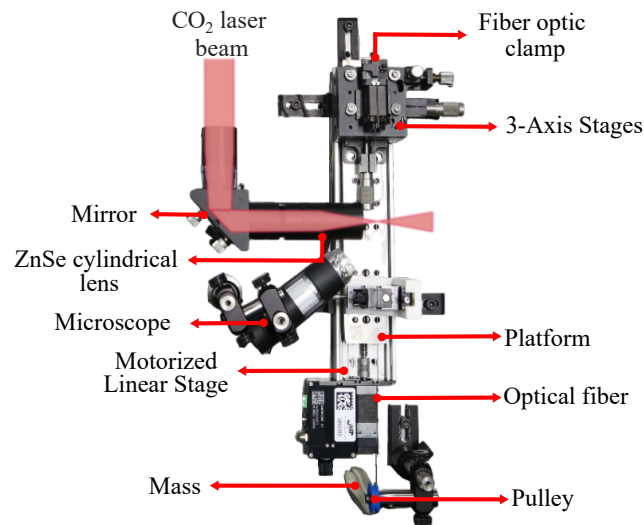


Figure 1. Experimental setup employed for the fabrication of LPFG-based modal converters written in few-mode optical fibers using the CO₂ laser technique.

After fabrication of the LPFG, its transmission spectrum was thoroughly evaluated using OptiGUI DataCollector software (v1.0) [40]. The characterization method includes a semiconductor tunable laser (APEX Technologies, AP3350A, Jacksonville, FL, USA) connected to one end of the LPFG, which allows the wavelength to be adjusted from 1526 nm to 1567 nm. This semiconductor optical source features a spectral width of only 300 kHz and a power stability of 0.05 dB @ 1 h, and guarantees a stable light polarization state in the tunable operating range. The other end of the LPFG was connected to a power meter (EXFO, PM-1600, Tokyo, Japan) in order to reconstruct the optical transmission spectrum; see Figure 2. As can be seen in the figure, the fabricated LPFG has a resonance around 1533.5 nm.

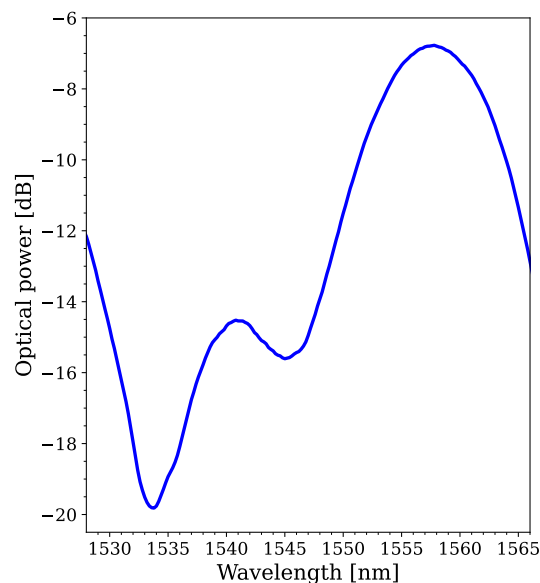


Figure 2. Transmission spectrum of the manufactured LPFG.

2.3. Setup for Mode Converter Characterization

To evaluate the potential of the LPFG inscribed in few-mode fiber as a platform for creating a mode converter device, the experimental setup depicted in Figure 3 was proposed,

which includes the semiconductor tunable laser described above. The laser emission was directed to the linear polarizer P1 in order to study how the modes responded when the light polarization was injected into the input of the modal converter with P1 at 0° or 90° . To ensure that the input mode was the fundamental mode, the laser was connected to a 0.5 m single-mode telecommunication optical fiber pigtail (SMF-28e, Corning, NY, USA). This optical fiber had a cutoff wavelength of 1260 nm and served the function of a mode filter, preventing higher-order modes at wavelengths near 1550 nm from being excited. This ensured that the mode at the input end of the fiber under test was LP_{01} . To preserve the polarization of the light after passing through the P1 polarizer, a lens focused the light beam on a 0.2 m section of PANDA fiber. Subsequently, this fiber section was spliced with the LPFG inscribed in the SM2000 optical fiber, as detailed in the previous section. It is worth noting that the proposed modal converter has a total length of 50 cm, and does not have the primary polymer coating because it was removed during the manufacturing process.

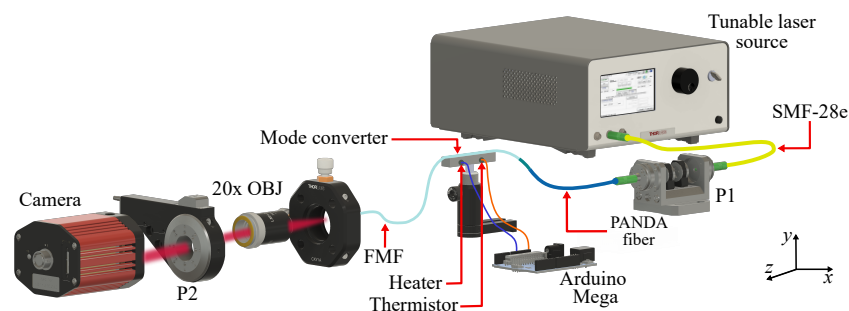


Figure 3. Experimental setup employed for characterization of the LPFG-based modal converters.

Next, a 20x objective lens was used at the output to collect the light emitted from the fiber core and produce a uniform wavefront. The light was transmitted through a second polarizer, known as the analyzer, which was placed in a motorized precision rotation stage (PRM1Z8, Thorlabs). This configuration allowed for incremental adjustment of the polarizer angle from 0° to 360° to assess the impact of the output polarization on the modal converter. Finally, a CCD camera (WiDy SWIR 640V-S, New Imaging Technologies, Paris, France) was employed to capture the image of the generated mode. To ensure the reliability and consistency of our tests, rigorous control over the laboratory environment was maintained. The temperature was kept constant at 20.62°C , while the humidity remained stable at 65%.

The configuration included a thermal control module specifically designed to ensure accurate temperature regulation. This module consisted of the hardware components required for closed-loop temperature control. The module employed an Arduino Mega 2560 (Arduino LLC, NY, USA), connected to a 12 V ceramic cartridge heater with a power rating of 40 W. The heater was responsible for heating the mode converter device using the RAMPS 1.4 power control board. A 100K NTC thermistor (Osensa Innovations Corp., BC, Canada), was used to obtain precise temperature measurements. The ceramic cartridge heater is housed in an aluminum block that surrounds the optical fiber, ensuring uniform heat distribution. On the other hand, an additional thermistor is placed inside the same block to enable real-time temperature monitoring. The monitoring process was facilitated using OptiGUI DataCollector software [40].

3. Data Description

The experimental setup illustrated in Figure 3 was employed to characterize a mode converter based on LPFG engraved in SM2000 optical fiber. The investigation of this mode converter was conducted at room temperature ($T_{room} = 20.62^\circ\text{C}$) and a fixed wavelength ($\lambda = 1534\text{ nm}$) to validate the mode conversion possibilities that this kind of device can offer. Then, the LP_{11} mode was injected into the mode converter under test along the horizontal axis (x -polarization). The light was captured by the CCD camera after passing through the mode converter, while the analyzer (P2) mounted on the rotational stage was

turned from 0° to 360° in increments of 1°. Figure 4a displays the recorded images. These results clearly demonstrate a mode conversion occurring at the output end, where the LP₁₁ mode transforms into the LP₀₁ mode at an angle of 87°. Furthermore, the results indicate that this device exhibits cyclic behavior as the analyzer completes 0° and 360° rotations.

Similarly, the experiment was repeated with the input light polarized along the vertical axis (*y*-polarization) using the P1 polarizer. Figure 4b shows the images obtained in this case. At the input of the mode converter, the LP₁₁ mode was again launched to the LPFG mode converter. In this case, as expected, the mode distribution is perpendicular to that obtained in the previous case. Moreover, it is evident again that rotating analyzer P2 at the output of the mode converter resulted in conversion from LP₁₁ mode to LP₀₁ mode.

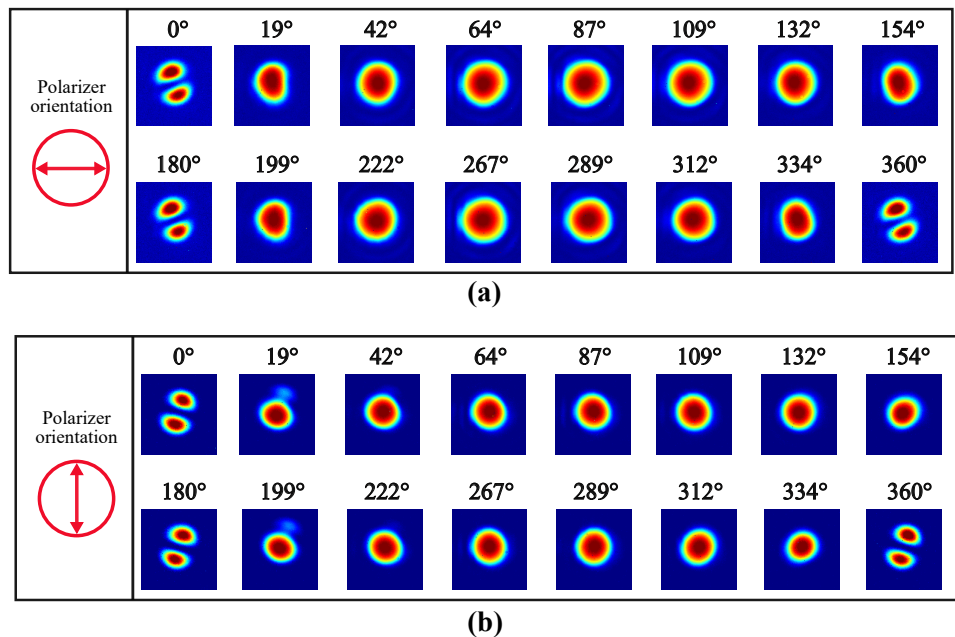


Figure 4. Modal converter operation. Intensity recorded by varying the angles of the analyzer (P2): (a) 0° and (b) 90°. Images were taken at room temperature and using a fixed wavelength of 1534 nm.

On the other hand, the wavelength of the optical source can influence the mode conversion of this type of device. For this reason, the experiment was repeated when this optical parameter was varied from 1527 nm to 1566 nm with 3 nm steps. Then, a folder with all recorded images was created. To simplify the identification of the CCD images, they were labeled according to the example provided in Figure 5. This label allows the three criteria of interest to be highlighted. The first parameter is the input polarization, which is limited to two options: 0 for horizontal polarization and 90 for vertical polarization. The second property of the label is the wavelength, which, as noted above, can range from 1527 nm to 1566 nm. Ultimately, the final component of the label denotes the polarization angle of the analyzer. Note that this parameter ranges from 0 (representing 0°) to 360 (representing 360°). For example, an image with the following label ModeLP-input_0deg-1555.0nm-output_120deg.tif corresponds to an image recorded with an input polarization of 0°, a wavelength equal to 1550.0 nm and an output polarization of 120°. On the other hand, it is important to note that all images were recorded in .tiff format to ensure the highest quality and to facilitate post-processing and analysis.

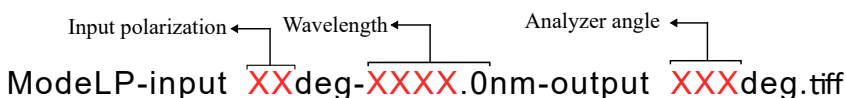
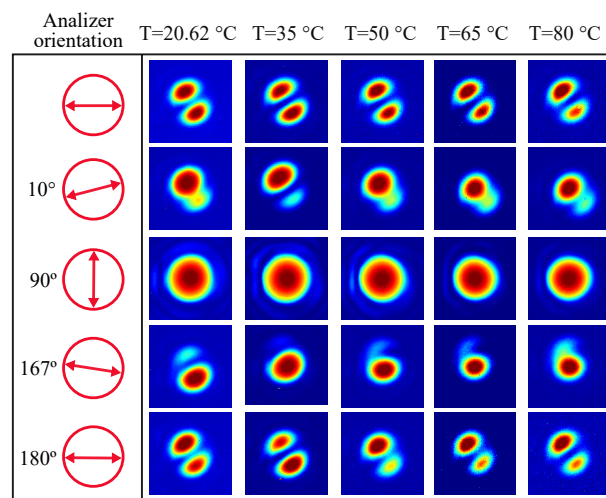
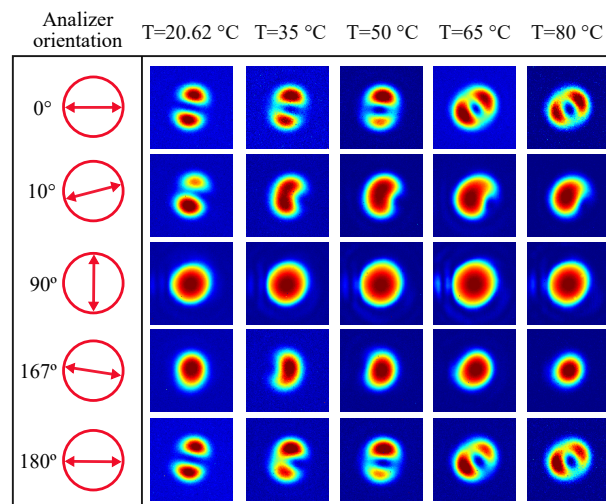


Figure 5. Nomenclature of the tiff images in the dataset. Note that the red text corresponds to the only elements that change in the file names (input polarization, wavelength, and output polarization).

Finally, the tunability of this mode converter was evaluated when an external temperature was applied. In this experiment, a heating system was employed to regulate temperature values. To accomplish this, an Arduino Mega was used for precise control, as explained in Section 2.3. This setup allowed us to maintain the desired temperature conditions throughout the experiment, ensuring the reliability and consistency of our results. More specifically, the analysis was performed at five distinct temperatures: 20.62 °C (room temperature), 35 °C, 50 °C, 65 °C, and 80 °C. Consequently, the investigation of the impact of changes in input polarization, output polarization, and wavelength was performed separately for each of the five temperatures. Figure 6 presents an example of the recordings acquired at a constant wavelength of 1527 nm. Figure 6a shows the behavior when the input mode is polarized at 0°. From these recordings, it is possible to observe that the mode conversion has a strong dependency on the output polarization and the applied temperature (the wavelength has an impact on the optical response as well, as evidenced in the dataset).



(a)

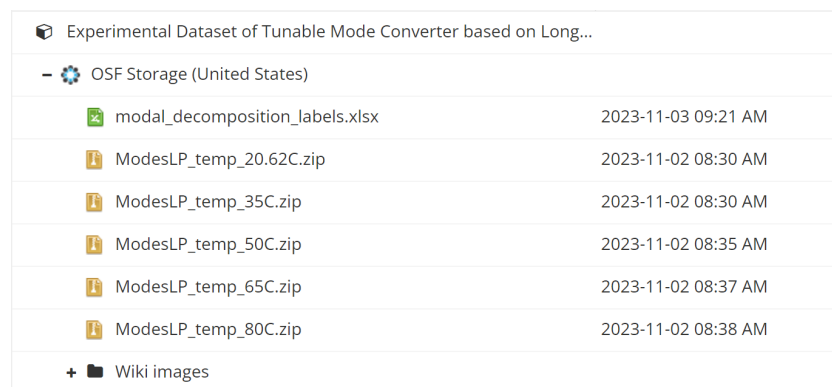


(b)

Figure 6. Near-field experimental patterns are obtained at the output end of the LPFG-based mode converter as a function of the applied temperature and analyzer angle when the polarization of the laser light at the input end of the device is aligned along the horizontal axis and the vertical axis. These results were obtained for a wavelength of 1527 nm while light was fed into the mode converter: (a) at 0° and (b) at 90°.

Similarly, Figure 6b shows the results obtained when the laser light polarization was along the horizontal axis, i.e., the input polarization was equal to 90° . The results show that when the temperature increases from 20.62°C to 80°C while holding the analyzer P2 at an angle of 10° , the modal conversion improves. It can be seen that the LP_{11} mode is transformed into the LP_{01} mode. The same happens when the analyzer is set to 0° and 180° . The transformation of the initial mode into a distinct intensity distribution is demonstrated. These results illustrate the accuracy of the results and show that the device is capable of modal conversion. It is important to note that having this database and evaluating the behavior of the modal converter allow the response of this type of device to be optimized using artificial intelligence techniques. As previously stated, the conversion is provided for specific experimental conditions; evaluating these manually is a complex and difficult task. Based on the above, the database reported in this work has a total of 49,736 images. As mentioned, this dataset shows the dependence of the LPFG-based mode converter on parameters such as input polarization, wavelength, output polarization, and applied temperature. Furthermore, the results provided in this work show that the modes at the output of the converter can be modified using the evaluated parameters, particularly when the temperature varies. This is mainly due to the thermo-optic effect, which causes changes in the refractive index, leading to variations in the resonance wavelength of the LPFG, as demonstrated above.

Figure 7 illustrates the structure of the repository. The root directory contains the file `modal_decomposition_label.xlsx`, which lists the labels of all images accompanied by the calculated parameters (the modal weight and phase of each obtained optical mode (LP_{01} , LP_{11a} , and LP_{11b})). We created a folder for each of the studied cases as well; thus, the root directory has five folders called `ModesLP_temp_20.62C`, `ModesLP_temp_35C`, `ModesLP_temp_50C`, `ModesLP_temp_65C`, and `ModesLP_temp_80C`. The database is accessible through the following link: <https://osf.io/3zk86/> (accessed on 29 December 2023).



Experimental Dataset of Tunable Mode Converter based on Long...		
- OSF Storage (United States)		
	modal_decomposition_labels.xlsx	2023-11-03 09:21 AM
	ModesLP_temp_20.62C.zip	2023-11-02 08:30 AM
	ModesLP_temp_35C.zip	2023-11-02 08:30 AM
	ModesLP_temp_50C.zip	2023-11-02 08:35 AM
	ModesLP_temp_65C.zip	2023-11-02 08:37 AM
	ModesLP_temp_80C.zip	2023-11-02 08:38 AM
+	Wiki images	

Figure 7. Summary of file location.

4. Modal Decomposition

One of the key applications of our imaging dataset lies in its fundamental contribution to modal decomposition. In this work, we propose an optimization algorithm for modal decomposition, supported by the obtained experimental data, that plays a crucial role in the extraction and analysis of propagation modes in FMF.

Efficient demultiplexing is crucial when transmitting light over a few-mode optical fiber to separate multiple signals sent through the same cable. Demultiplexing is achieved by two different methods. The first method involves physically separating modes using spatial light modulators, waveguides, low-coherence interferometry, or digital holography. These techniques require a substantial investment of resources to carry out experiments and perform intricate analysis of the collected data. The second technique relies on the utilization of numerical algorithms such as optimization procedures, Gerchberg–Saxton, and stochastic parallel gradient descent. The latter approach mainly involves the technique called Modal Decomposition (MD) [31,33,36,41]. This approach involves examining the

near-field intensity distributions of signals that have various modes. This is accomplished through an iterative update procedure that determines the intensities and phases of each individual eigenmode contained in the transmitted optical signal. To achieve this objective, the mathematical representation of the linear combination of all the eigenmodes can be defined as

$$U(r, \theta) = \sum_{n=1}^N \rho_n \exp(i\phi_n) \psi_n(r, \theta) \quad (5)$$

where $\psi_n(r, \theta)$ is the normalized field of the i^{th} eigenmode, N is the total number of eigenmodes, ϕ_n is the phase angle of the i^{th} eigenmode, and ρ_n is the amplitude (also known as the modal weight) of the i^{th} eigenmode. As shown in Figure 3, the modal intensity distribution can be recorded by the CCD camera, which is represented by $I(r, \theta)$ and is related to the near field through Equation (6).

$$I(r, \theta) \propto |U(r, \theta)|^2 \quad (6)$$

Here, it is important to emphasize that the phase of the fundamental mode can be considered as the reference, i.e., $\phi_1 = 0$. Furthermore, the phases are provided in the range of $[-\pi, \pi]$, and the fields are normalized. This results in

$$\sum_{n=1}^N (\rho_n)^2 = 1. \quad (7)$$

Therefore, the fundamental concept of the numerical MD method lies in determining the mode coefficient, which is essentially a combination of ϕ_n and ρ_n . At each iteration step, the modal weights and phases of the reconstructed mode are gradually adjusted until the shape similarity between the reconstructed beams and the measured beams reaches an acceptable level. To evaluate the agreement between the measured field and the reconstructed field, the use of the cross-correlation function from [33] is proposed:

$$C = \left| \frac{\iint \Delta I_{rec}(x, y) \Delta I_{med}(x, y) dx dy}{\sqrt{\iint \Delta I_{rec}^2(x, y) dx dy} \sqrt{\iint \Delta I_{med}^2(x, y) dx dy}} \right| \quad (8)$$

where $\Delta I_j(x, y) = I_j(x, y) - \bar{I}_j(x, y)$ and $\bar{I}_j(x, y)$ represents the mean value of the near-field intensity profile, with $j = r$ referring to the reconstructed profiles and $j = m$ to the measured profiles. The value of C is a parameter that varies between 0 and 1. When the reconstructed intensity profile perfectly matches the measured profile, as would be the case in a perfect modal decomposition, C equals 1. Conversely, when the images are entirely uncorrelated, C approaches a value near 0. To confront this issue, a particle swarm optimization (PSO) algorithm was used to assist in finding the best combinations of modal weights and relative phases that best matched the observed beam intensity.

To evaluate the potential usefulness of the produced database, the modal decomposition technique was used. Figure 8a shows an example of experimental intensity profiles with light is injected into the modal converter at 0° , the polarizer at the output set with angles corresponding to 0° , and a wavelength of 1534 nm. Along with the experimental intensity patterns, the patterns reconstructed by the DM algorithm are shown. Figure 8a shows the residual intensity profiles derived as $\Delta I = |I_{ORI} - I_{REC}|$ along with the corresponding correlation value. The results show a high degree of similarity between the reconstructed and experimental beam patterns with only minor residual intensity patterns, indicating that the suggested model is very accurate. It is worth noting that these results are remarkable considering that the images were obtained experimentally, whereas most works accomplish this type of analysis with computer-generated images [31,33,36,41].

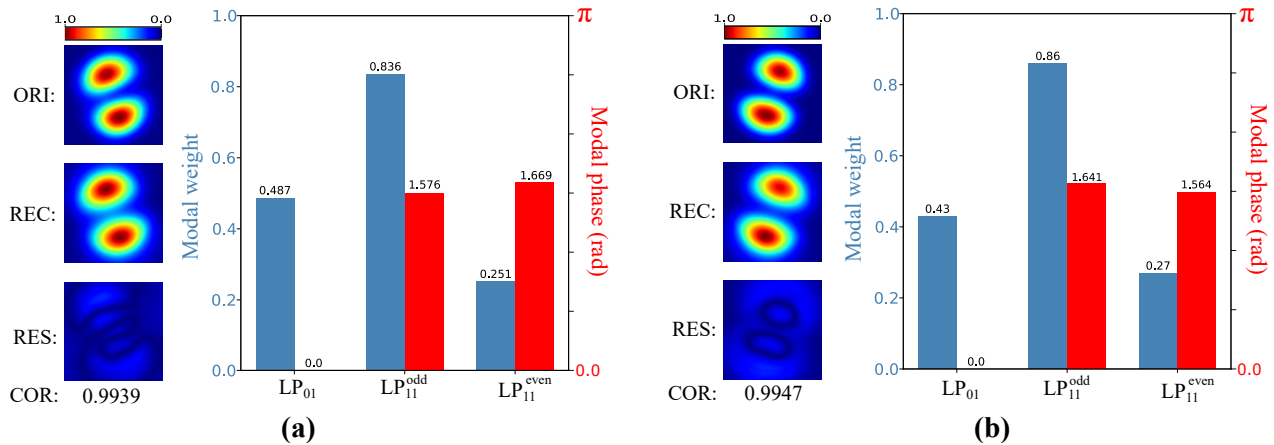


Figure 8. (a) Experimental (ORI) and reconstructed (REC) intensity profiles; (b) modal weights and relative phases for the intensity profiles.

The analysis was repeated by introducing light into the modal converter at a 90° angle while keeping the other variables fixed. The results are summarized in Figure 8b. It is important to note that the correlation coefficients for these two examples exceed 0.9930. As a complement, the consistently high correlation coefficients (above 0.9930) observed in both experiments reinforce the robustness and reliability of the modal decomposition technique across different injection angles. This level of correlation attests to the consistency and accuracy of the reconstructed beam patterns, affirming the versatility of the proposed model for various experimental configurations.

The proposed MD technique was implemented to quantify the weights (blue bars) and relative phases (red bars) for the obtained intensity profiles. There, it is evident that the produced modes contain components of the fundamental mode, the even LP₁₁, and the odd LP₁₁. Thus, the dominant mode in each recorded image can be detected using these levels, allowing for discrimination between the two LP₁₁ modes, which can be difficult to distinguish using only the collected intensity profile. For example, the images we examined clearly demonstrate a higher component of the odd LP₁₁. When light is polarized 0°, the weights of the LP₀₁, LP₁₁ odd, and LP₁₁ even modes are 0.487, 0.836, and 0.251, respectively. Similarly, the relative phases of these modes are 0.0, 1.576, and 1.669 radians. It should be noted that the absolute value of the relative phases was established by taking into account the opposing phase differences, which are unavoidable due to phase ambiguity, as discussed by Bruning et al. [42].

Finally, the MD method was employed to examine the changes in the amplitude of the LP₀₁ and LP₁₁ modes with an input polarization of 0°, the wavelength of 1534 nm, the temperature of 20.62°C, and the output polarization rotated from 0° to 360° as discussed above; see Figure 4. Figure 9 illustrates that the rotation of the P2 analyzer at the output of the mode converter causes a variation in the intensity of the mode, affecting the power reaching the camera sensor. The results indicate that the LP₀₁ mode exhibits a minimum modal weight when P2 is at 0°. However, as the analyzer is rotated, the modal weight of this mode gradually increases until a stable state is reached. In contrast, LP₁₁ mode exhibits the opposite behavior, starting with a maximum modal weight and gradually decreasing in value. Furthermore, it is evident that the modal weights show the anticipated cyclic pattern.

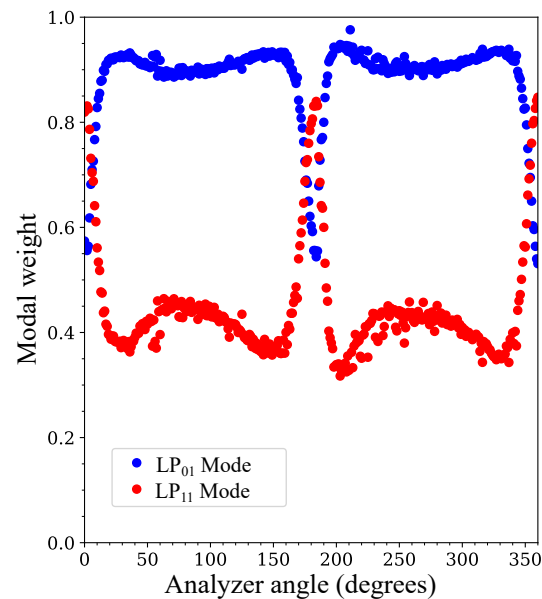


Figure 9. Comparison of the modal weight of the LP₀₁ and LP₁₁ modes as a function of the P2 analyzer angle. This analysis was performed for an input polarization of 0°, a wavelength of 1534 nm, and a temperature of 20.62 °C.

5. User Notes

Near-field intensity patterns are critical in the investigation of few-mode optical fibers because they allow the estimation of amplitude and phase information of the fiber eigenmodes at different wavelengths. This not only allows a complete study of the optical field and beam parameters, it provides vital insights into optical fiber anisotropy and polarization mode characterization. These aspects are critical for image processing in optical communication as well as deep learning analysis. It is much better to use mode datasets that were made experimentally from an all-fiber-optic-based modal converter than to use simulated data. These datasets represent the variability and inherent imperfections of real optical fibers obtained in real-world physical situations, such as temperature fluctuations, among others. Deep learning algorithms can now better adapt to real-world settings and solve problems that simulated data may ignore. Furthermore, the use of these datasets increases the ability to generalize the model and serves as a significant tool for validating and refining current theoretical models. In addition, depending on the specific objectives of the study, this dataset has the potential to be used in the context of exploring alternative neural network topologies, training approaches, and optimization methods. Among these alternatives are:

1. Users could apply different digital image processing techniques to extract essential information from the acquired images. The processed data could then be utilized to calculate the power associated with the specific mode under consideration. The quantification of mode power is crucial for assessing modal conversion efficiency, a fundamental parameter in the analysis of these devices.
2. Convolutional Neural Networks (CNNs) could be implemented to discover local patterns in images in order to classify optical modes according to the field distribution and analyze the quality of the obtained modes.
3. Generative networks could be used to generate new optical fiber modes or for data expansion. These techniques include the ability to generate additional modes that are not present in the original dataset. In fact, they technique can generate modes with patterns or characteristics comparable to real modes, increasing the variety of data accessible for training and testing deep learning models. Data expansion can contribute to improved generalization capacity of the model and help to improve the robustness of applications in optical fiber modal analysis.

4. Siamese networks can be used to compare optical fiber modes, as they are useful for learning similarities or differences between pairs of images.
5. Vision transformers are a novel class of models originally designed for computer vision tasks, but which have demonstrated remarkable adaptability in various domains, including optical fiber modal analysis. By considering these innovative architectures, we can harness the power of large datasets to further enhance the accuracy and efficiency of modal prediction and address a broader range of applications in the field.
6. Optimization algorithms can be implemented for modal decomposition.

All of these alternatives prove to be valuable tools for further improving the accuracy and efficiency of modal prediction while enabling a variety of tasks and applications, including classification, regression, and more.

Author Contributions: J.S.-P.: conceptualization, methodology, visualization, investigation, software, data curation, writing—review and editing. E.R.-V.: conceptualization, methodology, investigation, formal analysis, resources, data curation, writing—original draft, writing—review and editing, funding acquisition. J.M.-C.: investigation, data curation, formal analysis, writing—review and editing. P.T.: investigation, resources, supervision, writing—review and editing, formal analysis, project administration. All authors have read and agreed to the published version of the manuscript.

Funding: The authors acknowledge the support of the Instituto Tecnológico Metropolitano through project P20212 and the Universidad Nacional de Colombia through Hermes project 47472.

Institutional Review Board Statement: Not applicable.

Informed Consent Statement: Not applicable.

Data Availability Statement: Data regarding images and annotations can be accessed at the following repository: Experimental Dataset of Tunable Mode Converter based on Long-Period Fiber Gratings written in Few-mode Fiber: Impacts of Thermal, Wavelength, and Polarization Variations (direct URL <https://osf.io/3zk86/>).

Conflicts of Interest: The authors declare no conflicts of interest.

Abbreviations

The following abbreviations are used in this manuscript:

SDM	Spatial Division Multiplexing
SMF	Single-Mode Fiber
TMF	Two-Mode Fiber
LPG	Long-Period Grating
MCF	Multi-Core Fiber
OAM	Orbital Angular Momentum
CNN	Convolutional Neural Network
MUX	Multiplexers
DEMUX	Demultiplexers
TDM	Time Division Multiplexing
PDM	Polarization Division Multiplexing
MDM	Mode Division Multiplexing
LPFG	Long-Period Fiber Grating
MIMO	Multiple-Input Multiple-Output
FMF	Few-Mode optical Fiber
PC	Polarizer Controller
MD	Modal Decomposition

References

1. Montoya-Cardona, J.; Gomez-Cardona, N.; Gonzalez-Valencia, E.; Torres, P.; Reyes-Vera, E. Tunable Mode Converter Device Based on Photonic Crystal Fiber with a Thermo-Responsive Liquid Crystal Core. *Photonics* **2019**, *7*, 3. [[CrossRef](#)]
2. Park, K.J.; Song, K.Y.; Kim, Y.K.; Lee, J.H.; Kim, B.Y. Broadband mode division multiplexer using all-fiber mode selective couplers. *Opt. Express* **2016**, *24*, 3543. [[CrossRef](#)] [[PubMed](#)]

3. Leon-Saval, S.G.; Fontaine, N.K.; Salazar-Gil, J.R.; Ercan, B.; Ryf, R.; Bland-Hawthorn, J. Mode-selective photonic lanterns for space-division multiplexing. *Opt. Express* **2014**, *22*, 1036. [[CrossRef](#)] [[PubMed](#)]
4. Richardson, D.J.; Fini, J.M.; Nelson, L.E. Space-division multiplexing in optical fibres. *Nat. Photonics* **2013**, *7*, 354–362. [[CrossRef](#)]
5. Tkach, R.W. Scaling optical communications for the next decade and beyond. *Bell Labs Tech. J.* **2010**, *14*, 3–9. [[CrossRef](#)]
6. Puttnam, B.J.; Rademacher, G.; Luís, R.S. Space-division multiplexing for optical fiber communications. *Optica* **2021**, *8*, 1186. [[CrossRef](#)]
7. Martelli, P.; Gatto, A.; Boffi, P.; Martinelli, M. Free-space optical transmission with orbital angular momentum division multiplexing. *Electron. Lett.* **2011**, *47*, 972. [[CrossRef](#)]
8. Correa-Rojas, N.; Gallego-Ruiz, R.; Álvarez Castaño, M. Generation of linearly polarized modes using a digital micromirror device and phase optimization. *Comput. Opt.* **2022**, *46*, 30–38. [[CrossRef](#)]
9. Zou, K.; Pang, K.; Song, H.; Fan, J.; Zhao, Z.; Song, H.; Zhang, R.; Zhou, H.; Minoofar, A.; Liu, C.; et al. High-capacity free-space optical communications using wavelength- and mode-division-multiplexing in the mid-infrared region. *Nat. Commun.* **2022**, *13*, 7662. [[CrossRef](#)]
10. El-Nahal, F.; Xu, T.; AlQahtani, D.; Leeson, M. A Bidirectional Wavelength Division Multiplexed (WDM) Free Space Optical Communication (FSO) System for Deployment in Data Center Networks (DCNs). *Sensors* **2022**, *22*, 9703. [[CrossRef](#)]
11. Galvis-Arroyave, J.; Villegas-Aristizabal, J.; Montoya-Cardona, J.; Montoya-Villada, S.; Reyes-Vera, E. Experimental characterization of a tuneable all-fiber mode converter device for mode-division multiplexing systems. *J. Phys. Conf. Ser.* **2020**, *1547*, 012004. [[CrossRef](#)]
12. Montoya-Cardona, J.; Gomez-Cardona, N.; Gonzalez-Valencia, E.; Torres, P.; Reyes-Vera, E. Tuneable liquid crystal asymmetric dual-core photonic crystal fiber mode converter. *J. Phys. Conf. Ser.* **2020**, *1547*, 012008. [[CrossRef](#)]
13. Skorobogatiy, M.; Anastassiou, C.; Johnson, S.; Weisberg, O.; Engeness, T.; Jacobs, S.; Ahmad, R.; Fink, Y. Quantitative characterization of higher-order mode converters in weakly multimoded fibers. *Opt. Express* **2003**, *11*, 2838. [[CrossRef](#)] [[PubMed](#)]
14. Zhang, X.; Liu, Y.; Wang, Z.; Yu, J.; Zhang, H. LP₀₁-LP_{11a} mode converters based on long-period fiber gratings in a two-mode polarization-maintaining photonic crystal fiber. *Opt. Express* **2018**, *26*, 7013. [[CrossRef](#)] [[PubMed](#)]
15. Gao, Y.; Sun, J.; Chen, G.; Sima, C. Demonstration of simultaneous mode conversion and demultiplexing for mode and wavelength division multiplexing systems based on tilted few-mode fiber Bragg gratings. *Opt. Express* **2015**, *23*, 9959. [[CrossRef](#)] [[PubMed](#)]
16. Cai, S.; Yu, S.; Wang, Y.; Lan, M.; Gao, L.; Gu, W. Hybrid Dual-Core Photonic Crystal Fiber for Spatial Mode Conversion. *IEEE Photonics Technol. Lett.* **2016**, *28*, 339–342. [[CrossRef](#)]
17. Witkowska, A.; Leon-Saval, S.G.; Pham, A.; Birks, T.A. All-fiber LP₁₁ mode converters. *Opt. Lett.* **2008**, *33*, 306. [[CrossRef](#)]
18. Jin, W.; Chiang, K.S. Mode converters based on cascaded long-period waveguide gratings. *Opt. Lett.* **2016**, *41*, 3130. [[CrossRef](#)]
19. Yang, Y.; Chen, K.; Jin, W.; Chiang, K.S. Widely Wavelength-Tunable Mode Converter Based on Polymer Waveguide Grating. *IEEE Photonics Technol. Lett.* **2015**, *27*, 1985–1988. [[CrossRef](#)]
20. Chen, G.; Zhang, R.; Sun, J. On-chip optical mode conversion based on dynamic grating in photonic-phononic hybrid waveguide. *Sci. Rep.* **2015**, *5*, 10346. [[CrossRef](#)]
21. Reyes-Vera, E.; Usuga-Restrepo, J.; Gómez-Cardona, N.; Varón, M. *Mode Selective Coupler Based in a Dual-Core Photonic Crystal Fiber with Non-Identical Cores for Spatial Mode Conversion*; OSA: Washington, DC, USA, 2016; p. LTu3C.1. [[CrossRef](#)]
22. Sakata, H.; Sano, H.; Harada, T. Tunable mode converter using electromagnet-induced long-period grating in two-mode fiber. *Opt. Fiber Technol.* **2014**, *20*, 224–227. [[CrossRef](#)]
23. Zhao, Y.; Liu, Y.; Zhang, L.; Zhang, C.; Wen, J.; Wang, T. Mode converter based on the long-period fiber gratings written in the two-mode fiber. *Opt. Express* **2016**, *24*, 6186. [[CrossRef](#)] [[PubMed](#)]
24. Liu, Z.; Zhao, X.; Mou, C.; Liu, Y. Mode Selective Conversion Enabled by the Long-Period Gratings Inscribed in Elliptical Core Few-Mode Fiber. *J. Light. Technol.* **2020**, *38*, 1536–1542. [[CrossRef](#)]
25. Fei, Y.; Xu, Y.; Huang, D.; Dong, Y.; Zhang, B.; Ni, Y.; Wai, P.K.A. On-Chip Reconfigurable and Ultracompact Silicon Waveguide Mode Converters Based on Nonvolatile Optical Phase Change Materials. *Nanomaterials* **2022**, *12*, 4225. [[CrossRef](#)] [[PubMed](#)]
26. Igarashi, K.; Souma, D.; Takeshima, K.; Tsuritani, T. Selective mode multiplexer based on phase plates and Mach-Zehnder interferometer with image inversion function. *Opt. Express* **2015**, *23*, 183. [[CrossRef](#)] [[PubMed](#)]
27. Zhao, W.; Liu, R.; Peng, Y.; Yi, X.; Chen, H.; Dai, D. High-performance silicon polarization switch based on a Mach-Zehnder interferometer integrated with polarization-dependent mode converters. *Nanophotonics* **2022**, *11*, 2293–2301. [[CrossRef](#)]
28. Wang, W.; Wu, J.; Chen, K.; Jin, W.; Chiang, K.S. Ultra-broadband mode converters based on length-apodized long-period waveguide gratings. *Opt. Express* **2017**, *25*, 14341. [[CrossRef](#)]
29. Liu, S.; Zhang, Y.; Fu, C.; Bai, Z.; Li, Z.; Liao, C.; Wang, Y.; He, J.; Liu, Y.; Wang, Y. Temperature Insensitivity Polarization-Controlled Orbital Angular Momentum Mode Converter Based on an LPFG Induced in Four-Mode Fiber. *Sensors* **2018**, *18*, 1766. [[CrossRef](#)]
30. Zheng, Y.; Guo, H.; Feng, M.; Wang, Z.; Liu, Y. Wavelength-Tunable, Ultra-Broadband, Biconical, Long-Period Fiber Grating Mode Converter Based on the Dual-Resonance Effect. *Sensors* **2021**, *21*, 5970. [[CrossRef](#)]
31. Manuylovich, E.S.; Dvoyrin, V.V.; Turitsyn, S.K. Fast mode decomposition in few-mode fibers. *Nat. Commun.* **2020**, *11*, 5507. [[CrossRef](#)]
32. Shapira, O.; Abouraddy, A.F.; Joannopoulos, J.D.; Fink, Y. Complete Modal Decomposition for Optical Waveguides. *Phys. Rev. Lett.* **2005**, *94*, 143902. [[CrossRef](#)] [[PubMed](#)]

33. Yan, B.; Zhang, J.; Wang, M.; Jiang, Y.; Mi, S. Degenerated mode decomposition with convolutional neural network for few-mode fibers. *Opt. Laser Technol.* **2022**, *154*, 108287. [[CrossRef](#)]
34. Yan, W.; Xu, X.; Wang, J. Modal decomposition for few mode fibers using the fractional Fourier system. *Opt. Express* **2019**, *27*, 13871. [[CrossRef](#)] [[PubMed](#)]
35. Yao, Q.; Yang, H.; Zhu, R.; Yu, A.; Bai, W.; Tan, Y.; Zhang, J.; Xiao, H. Core, Mode, and Spectrum Assignment Based on Machine Learning in Space Division Multiplexing Elastic Optical Networks. *IEEE Access* **2018**, *6*, 15898–15907. [[CrossRef](#)]
36. Huang, L.; Guo, S.; Leng, J.; Lü, H.; Zhou, P.; Cheng, X. Real-time mode decomposition for few-mode fiber based on numerical method. *Opt. Express* **2015**, *23*, 4620. [[CrossRef](#)] [[PubMed](#)]
37. Xu, M.; Hou, M.; Luo, X.; Xu, J.; Chen, W.; An, Y.; Zeng, X.; Li, J.; Huang, L. Multi-order hybrid vector mode decomposition in few-mode fibers with DL-based SPGD algorithm. *Opt. Laser Technol.* **2023**, *167*, 109795. [[CrossRef](#)]
38. Lee, D.L. *Electromagnetic Principles of Integrated Optics*; Wiley: Hoboken, NJ, USA, 1986.
39. Valencia-Garzón, S.; Reyes-Vera, E.; Galvis-Arroyave, J.; Montoya, J.P.; Gomez-Cardona, N. Metrological Characterization of a CO₂ Laser-Based System for Inscribing Long-Period Gratings in Optical Fibers. *Instruments* **2022**, *6*, 79. [[CrossRef](#)]
40. Soto-Perdomo, J.; Morales-Guerra, J.; Arango, J.; Montoya-Villada, S.; Torres, P.; Reyes-Vera, E. OptiGUI DataCollector: A graphical user interface for automating the data collecting process in optical and photonics labs. *SoftwareX* **2023**, *24*, 101521. [[CrossRef](#)]
41. An, Y.; Li, J.; Huang, L.; Li, L.; Leng, J.; Yang, L.; Zhou, P. Numerical mode decomposition for multimode fiber: From multi-variable optimization to deep learning. *Opt. Fiber Technol.* **2019**, *52*, 101960. [[CrossRef](#)]
42. Brüning, R.; Gelszinnis, P.; Schulze, C.; Flamm, D.; Duparré, M. Comparative analysis of numerical methods for the mode analysis of laser beams. *Appl. Opt.* **2013**, *52*, 7769. [[CrossRef](#)]

Disclaimer/Publisher’s Note: The statements, opinions and data contained in all publications are solely those of the individual author(s) and contributor(s) and not of MDPI and/or the editor(s). MDPI and/or the editor(s) disclaim responsibility for any injury to people or property resulting from any ideas, methods, instructions or products referred to in the content.